# In vitro Raman imaging of human macrophages: Impact of eicosapentaenoic acid on the hydrolysis of cholesterol esters in lipid droplets

Ali Muhieddine, Natalie Fournier, Hani Dakroub, Ali Assi, Jean-Louis Paul, Ali Tfayli, Pierre Chaminade, Sana Tfaili

▶ **To cite this version:**

Ali Muhieddine, Natalie Fournier, Hani Dakroub, Ali Assi, Jean-Louis Paul, et al.. In vitro Raman imaging of human macrophages: Impact of eicosapentaenoic acid on the hydrolysis of cholesterol esters in lipid droplets. Talanta, 2023, 256, pp.124314. 10.1016/j.talanta.2023.124314 . hal-04528241

**HAL Id: hal-04528241**
**https://hal.science/hal-04528241**

Submitted on 2 Apr 2024

**HAL** is a multi-disciplinary open access archive for the deposit and dissemination of scientific research documents, whether they are published or not. The documents may come from teaching and research institutions in France or abroad, or from public or private research centers.

L'archive ouverte pluridisciplinaire **HAL**, est destinée au dépôt et à la diffusion de documents scientifiques de niveau recherche, publiés ou non, émanant des établissements d'enseignement et de recherche français ou étrangers, des laboratoires publics ou privés.

# In vitro Raman imaging of human macrophages: impact of eicosapentaenoic acid on the hydrolysis of cholesterol esters in lipid droplets

Ali Muhieddine[a], Natalie Fournier[b], Hani Dakroub[b], Ali Assi[a], Jean-Louis Paul[b], Ali Tfayli[a], Pierre Chaminade[a], and Sana Tfaili[a*]

[a] Lip(Sys)² - Chimie Analytique Pharmaceutique, UFR Pharmacie, Université Paris-Saclay, Orsay, France
[b] Lip(Sys)² - Equipe de Biologie, UFR Pharmacie, Université Paris-Saclay, Orsay, France

***Corresponding author** Sana Tfaili

**Email :** sana.tfaili@universite-paris-saclay.fr

**Postal address** Lip(Sys)² - Faculté de Pharmacie - Université Paris Saclay –Bâtiment Henri Moissan - 17, avenue des sciences – 91400 Orsay - France

## Abstract

Atherosclerosis – a cardiovascular disease and the primary cause of morbidity and mortality in industrialized countries – is linked to the existence of atherosclerotic plaques characterized by cholesterol-laden macrophages called foam cells. In these cells, cholesterol esters associated with triglycerides form lipid droplets (LD). The only way to remove this excess cholesterol is to promote free cholesterol efflux from macrophages to specific acceptors. It has been shown recently that eicosapentaenoic acid (EPA) reduces efflux on cholesterol-loaded THP-1 macrophages *in vitro* due to decreased cholesterol esters hydrolysis. These *in vitro* observations could reflect EPA's difficulty in facilitating *in vivo* the antiatherogenic process of cholesterol efflux within advanced atherosclerotic plaques.

This work aims to study *in vitro* the impact of EPA on cholesterol esters hydrolysis in the LD of human THP-1 macrophages using vibrational Raman microspectroscopy. For this, we used deuterated EPA and recorded spectral images at the cell scale after different hydrolysis times.

Results showed that EPA is involved in forming triglycerides and phospholipids of LD. Hydrolysis kinetics slowed down after 24 hours, triglycerides increased, and the intensity of the characteristic bands linked to deuteration decreased. The size of LD without hydrolysis (H0) is higher than that after 24h (H1) or 48h (H2) of hydrolysis. The size decrease is sharper when going from H0 to H1 than from H1 to H2. Principal component analysis illustrated data' projection according to the cellular compartment, the hydrolysis time, and the supplementation of the medium.

**Keywords**

Raman imaging, Lipid droplets, Vibrational spectroscopy, Chemometrics, THP-1 macrophages, Atherosclerosis

## 1. Introduction

Cardiovascular diseases (CVD) represent a significant cause of morbidity and mortality in industrialized countries. CVDs result from atherosclerotic plaques characterized by cholesterol-laden macrophages (foam cells). In these cells, cholesterol esters (CE) are associated with triglycerides (TG) and form voluminous lipid droplets (LD) [1]. The only way to eliminate this excess of cholesterol is to promote the efflux or outflow of free cholesterol (FC) from macrophages towards HDL or pre-β HDL type acceptors. CE hydrolysis – carried out by the cytoplasmic enzyme nCEH (neutral cholesterol ester hydrolase) – is the essential preliminary step to efflux, and its predominant mechanism involves the membrane transporter ABCA1 (ATP-binding cassette A1) [2]. Recently, the clinical study REDUCE-IT confirmed the cardioprotective role of eicosapentaenoic acid (EPA, 20:5 n-3), a polyunsaturated fatty acid from the omega 3 family (n-3 PUFA) [3]. However, despite widely documented anti-inflammatory effects, the mechanisms by which n-3 PUFAs exert this effect are not fully understood [4]. To learn more about the impact of PUFAs, the three main PUFAs: eicosapentaenoic acid (EPA, 20:5 n-3), arachidonic acid (AA, 20:4 n-6), and docosahexaenoic acid (DHA, 22:6 n-3) have been studied on different cell lines. According to the literature, the *in vitro* impact on free cholesterol efflux varies according to the added PUFA. This impact also varies according to cell type (murine or human macrophages, continuous line or cells in primary culture) and the cholesterol content of the macrophages. Studies reported that EPA increases ABCA1-dependent efflux (+28%) from cholesterol-normal THP-1 macrophages, while AA and DHA have no effect at the tested concentrations [5]. This cardioprotective effect observed *in vitro* is consistent with epidemiological studies objectifying the positive impact of EPA on CVD. Conversely, EPA reduces ABCA1 efflux (-17%) from cholesterol loaded THP-1 macrophages, while AA and DHA have no impact (unpublished results). Moreover, we have experimental data strongly suggesting that the decreased FC efflux caused by EPA is the consequence of a decrease in CE hydrolysis. Indeed, we conducted some experiments using an ACAT inhibitor added during the cholesterol-loading period and maintained during the subsequent steps. These conditions allowed obtaining FC-enriched cells. When THP-1 macrophages were FC-loaded, the EPA supplementation did not reduce the isotopic cholesterol efflux mediated by ABCA-1. These *in vitro* observations could reflect the i*n vivo* inability of EPA to facilitate the antiatherogenic process of cholesterol efflux from foam cells within atheroma [6].

We hypothesize that the mechanism, by which EPA – unlike the other PUFAs – reduces the hydrolysis of the CE of the LDs of foam human THP-1 cells, involves modifications in the fatty acid composition of intracellular lipids. To confirm this hypothesis, we aim to learn about the impact of EPA on the efflux of cholesterol-loaded macrophages THP-1 using Raman spectroscopy.

Raman spectroscopy is known for its great potential in cell analysis due to its chemical specificity and ability to be applied to a small number of cells or even a single cell in a non-destructive way [7]. Several studies proved the feasibility of Raman microspectroscopy in cell analysis. Using Raman imaging, Majzner, et al., studied the impact of supplementation with

arachidonic acid (AA) and eicosapentaenoic acid (EPA) – in the presence or absence of 1-methylnicotinamide (MNA) ions – on the formation of LD in human endothelial cells. The authors compared the degree of unsaturation of the LDs by calculating the bands' ratio of ν C=C / ν $CH_2$ (1656 / 1444 $cm^{-1}$) The ratio value associated with LD spectra of cells supplemented with AA was similar to that of the raw AA molecule's spectrum. The authors reached the same conclusion for EPA. This indicates that LDs are rich in PUFAs due to their uptake by human endothelial cells. Using 3D images, they determined the LDs' location, number, and dimensions. Cells supplemented with MNA were characterized by many LDs, which means that MNA facilitates the transport of PUFAs into the cytoplasm, leading to more LDs [8].

Stiebing et al., followed the kinetics of incorporating d8-arachidonic acid into THP-1 macrophages and a mixture of d-31 palmitic acid and d8-arachidonic acid by Raman vibrational imaging [9]. Deuteration facilitated AA tracking due to the shift of the ν CH and ν $CH_2$ bands into ν CD and ν $CD_2$ bands. Foam cells were formed until saturation after 8 hours of incubation with deuterated AA. While this formation of LDs is detected after 24 h of incubation for palmitic and oleic acid. The authors explain this result by the fact that AA would be stored in the LDs but also metabolized in other cellular compartments, for example, into phospholipids. The difference in the synthesis of deuterated molecules allows following characteristic bands for d-31 palmitic acid (2100 and 2197 $cm^{-1}$) and d8-arachidonic acid (2248 $cm^{-1}$). Facing the mixture, LDs were formed continuously with a heterogeneous fatty acid composition. Palmitic acid is stored homogeneously in the LDs, but AA is stored in the LDs and other compartments as already specified [9]. In another study, Stiebing et al., followed by Raman imaging the endocytosis of oxidized LDL by THP-1 [7]. The particularity lies in deuterated tripalmitate (d-TP) in isolated LDL. Understanding the endocytic pathway and the intracellular fate of modified lipoproteins is of primary interest in the development of atherosclerosis. The increase in signals between 2000 and 2300 $cm^{-1}$ appeared after 72 hours only and confirmed the presence of d-TP in the LDs. In addition, the presence of a constituent of LDL – beta carotene (ν C=C at 1519 $cm^{-1}$ and ν C-C 1155 $cm^{-1}$) – has been confirmed in LD. Typically, macrophages in conventional cell culture do not contain beta carotene. This allows it to be used as an LDL marker [7].

Matthäus et al., studied the metabolism of two fatty acids (d-31palmitic acid and d-33 oleic acid) and d6-2,2,3,4,4,6 cholesterol in THP-1 cells. The intensity ratio of CD/CH (2050−2275 $cm^{-1}$/ 2800−3020 $cm^{-1}$) increased over time for both fatty acids [10]. This confirms that fatty acids are progressively stored in the form of triglycerides in LDs. A quantitative exponential model was established to calculate the concentration of their storage. Incubation beyond 40 hours leads to the death of cells due to lipotoxicity. On the other hand, the incubation of THP-1 in the presence of deuterated cholesterol showed a CD/CH ratio increasing in LD. However, this ratio is lower compared to fatty acids since cholesterol undergoes efflux. Unlike fatty acids, incubation in the presence of cholesterol did not lead to cell death during the 72 h [10].

Tfaili et al., tracked murine J774 macrophages under different supplementation conditions using Raman and infrared (IR) vibrational imaging [11]. Modifications in lipid composition and intensity have been highlighted. Cells loaded with acetylated LDL and supplemented with

EPA showed more intense lipid distribution than unloaded media. The possibility of recording spectra at the LD level was underlined as well as the contribution of chemometric tools. Indeed, the chemometric tools managed to discriminate between the nucleus and the cytoplasm in Raman and in IR (although in IR, the pixel of the image essentially covers a cell); and to discriminate between the four culture conditions. The contribution of vibrational techniques for the monitoring of intracellular LD seemed promising; especially in Raman as the LD were clearly visible under the microscope [11].

The interest of vibrational spectroscopy for monitoring the incorporation of lipids and PUFAs in the formation of droplets is well established now. Our study aims to investigate the lipid modifications on THP-1 macrophages in different cell growth conditions relying on deuterium labeling of EPA and on chemometric tools. This work was carried out using THP-1 human macrophages, a genetically homogenous cell line whose culture is easy and which offers the advantage of providing a large amount of cellular material in a short time compared to the HMDM human cell line [12,13]. After mimic of foam cells observed *in vivo* in the atherosclerotic plaques, our aim is to study *in vitro* the impact of EPA on the efflux of cholesterol-loaded macrophages THP-1 by using Raman spectroscopy. We studied different cell conditions: THP-1 cells loaded with acetylated LDL in a standard medium (not supplemented culture medium), or in a supplemented medium with EPA or with EPA-d5, without or with applying a time for hydrolysis of acetylated LDL after the last phase of cell preparation. The Raman spectral signature of THP-1 under different culture conditions allows associating the molecular information with the spatial distribution. These analyses also permit the evaluation of the number, size, and location of the LDs on the fixed cells. The use of deuterated EPA facilitates its monitoring, and the chemometric tools help in highlighting modifications of spectral signature according to the culture conditions.

## 2. Materials and methods

### 2.1. Preparation of the samples for subsequent analyses by Raman spectroscopy

#### 2.1.1. THP-1 cell culture

A vial of frozen THP-1 human monocytes cell line purchased from American Type Culture Collection–(ATCC, Manassas, VA) was thawed in a 75 $cm^2$ flask containing the culture medium and placed at 37°C under 5% $CO_2$. This culture medium contains RPMI-1640 medium supplemented with 20% heat-inactivated fetal bovine serum (FBS) (Thermo Fisher Scientific, Germany), 2mM L-Glutamine, 100 U/mL penicillin-streptomycin (PS), and 10 mM HEPES. One week after this step, the cells were maintained in the same medium called complete culture medium but with only 10% FBS instead of 20%.

For our experiments, monocytes were seeded in Primaria® 6-well plates (9.6 $cm^2$/well) in the complete medium supplemented with 10% FBS. In order to stimulate the differentiation of monocytes into macrophages, monocytes were incubated with 100 nM of phorbol-12-myristate-13-acetate (PMA) (Sigma-Aldrich, Saint-Quentin Fallavier, France) for 72 h.

### 2.1.2. Preparation of acetylated LDL

LDL was isolated from the plasma of individual donors (Etablissement Français du Sang, EFS) by ultracentrifugation in the density range of 1.019-1.063 g/mL. Native LDL was chemically modified by acetylation (acLDL) with the use of a solution of sodium acetate and acetic anhydride [Basu SK 2016 PNAS]. Under soft stirring and on a bed of ice, 2 mg of LDL are acetylated by adding volume to volume of a saturated solution of sodium acetate and 10 µL of acetic anhydride (repeated additions of 2 µL spaced 10 minutes apart). After dialysis against PBS and filtration on 0.2 µM, acLDL was stored at 4 °C and used within two weeks. The increase in relative electrophoretic mobility on agarose gel confirmed the success of acLDL preparation.

### 2.1.3. Growing of cells in standard or EPA-supplemented media

During cell culture, it is necessary to determine the cell density to adjust it to the required level for seeding (400 x $10^4$ cells / mL). This optimal value was defined according to the dimension of the wells and the duration of the culture.

The cells were then seeded on a $CaF_2$ slide in each well. Macrophages were seeded in 2 mL of complete culture medium (10% FBS) per well (800 x $10^4$ cells/well). After 72 h, this complete culture medium was replaced by complete media (10% FBS) supplemented or not with fatty acids (FAs). The first well was replaced by standard (STD) medium, the second well was replaced by medium supplemented with eicosapentaenoic acid (EPA) (Cayman Chemical Company, Ann Harbor, MI) at 70 µM, and the third well was replaced by medium supplemented with deuterated eicosapentaenoic acid (EPA-d5) (Larodan Fine chemicals, Sweden) at 70 µM.

### 2.1.4. Cholesterol overloading of cells by acetylated LDL

After 72 h, the media were replaced by 1.5 mL of the culture media (RPMI 1640, L-glutamine, PS, and HEPES) supplemented or not with EPA or EPA-d5 without FBS (so-called incomplete medium) and containing 0.2% bovine serum albumin (BSA). During this step, acetylated LDL was added to these experimental media at a concentration of 150 µg/mL to ensure the cholesterol overloading of the cells. PMA must be maintained in each well during all these stages in order to maintain the full differentiation of monocytes into macrophages.

### 2.1.5 Addition of LXR/RXR system agonists

After 30 h of incubation with acLDL, the cells were equilibrated in an incomplete medium containing 0.2% BSA and LXR/RXR agonists (5 µg/mL of 22-hydroxy-cholesterol and 10 µM of 9 cis-retinoic acid) to stimulate the expression of the ABCA1 transporter. This step, which lasts about 16 hours, mimics the operating conditions used to measure cholesterol efflux.

### 2.1.6 Hydrolysis of cholesteryl esters (CE)

After the equilibration step, three $CaF_2$ slides, each from one of the STD, EPA and EPA-d5 media, were analyzed immediately before the triggering of the hydrolysis of the CE, which corresponds to the hydrolysis time called t0. In parallel, six other slides, 2 of which come from each cellular condition, were incubated for 24 h and six others for 48 h in an incomplete culture medium supplemented with 5 µg/mL of an ACAT inhibitor (*Acyl CoenzymeA Acyl Transferase*) to prevent any re-esterification of free cholesterol generated by the hydrolysis of CE.

### 2.1.4. Fixing cells on the $CaF_2$ windows

$CaF_2$ slides were delicately picked up from the wells. Cells were incubated with 2–3 mL of 4% paraformaldehyde (PFA) for 15 min. The PFA was then aspirated, and the $CaF_2$ windows were washed with PBS and then distilled water. The first washing with 1.5–2 mL PBS eliminates the culture medium. Three washes with distilled water by filling 2/3 of the wells follow to prevent the deposition of PBS crystals.

## 2.2. Raman vibrational spectroscopy analysis

Raman data are recorded via the Labspec 6 software on a Labram HR microspectrometer (Horiba Scientific, France SAS Villeneuve d'Ascq). The microspectrometer is equipped with an excitation He:Ne laser source operating at a 632.81 nm excitation source (Toptica Photonics, Munich, Germany), a CCD detector (1024 × 256 pixels) and a long focal microscope objective X100 LF with a numerical aperture NA of 0.9 (Olympus, Tokyo, Japan). The confocal pinhole was set at 200 µm and the slit aperture at 300 µm. A grating of 300 grooves/mm permitted to collect data with a spectral resolution of 4 $cm^{-1}$. The acquisition time was set to 5 seconds with 4 accumulations on the interval 400-4000 $cm^{-1}$, so the acquisition time of a spectrum last 1.5 minutes.

### 2.2.1. Acquisition of EPA and EPA-d5 spectral signature

50 µL of EPA and EPA-d5 were deposited on two $CaF_2$ slides separately and then air-dried. 6 spectra are recorded per slide, and then the type of vibrational bands was assigned on the mean standardized EPA and EPA-d5 spectra.

### 2.2.2. Raman image acquisition of THP-1 macrophages

Using the same device and via a motorized stage, Raman images were recorded. The step was set to 1 µm, and the autofocus on each point was activated. Three images of cells were recorded per slide (45 images in total). The duration of acquisition depended on the cell size.

### 2.2.3. Extraction of spectra of nuclei, cytoplasm, and lipid droplets

The spectral signatures of nuclei (10 spectra per cell), cytoplasms (10 spectra per cell), and all lipid droplets present in each cell were extracted from the spectral images. The corresponding size of the lipid droplets was measured in µm using the visible image. For each cell, the average spectrum of the spectra of nuclei, cytoplasm, and the present droplets was then calculated.

## 2.3. Data processing

A smoothing and correction of the baseline were carried out via Labspec 6 for all the data:

- A Savitzky-Golay smoothing, polynomial type, for a degree of 3 and a window of 12 points, and a manual correction of the baseline were performed on the EPA and EPA-d5 spectra.
- A "DeNoise" type smoothing for a factor of 3 and a window of 5 points and a correction of the polynomial baseline with a degree of 3 and a window of 27 points were carried out on the spectral images.

SNV (*Standard Normal Variate*) standardization was performed on the average spectra before band assignment.

Finally, a Principal Component Analysis (PCA) was performed based on the SAISIR package in Matlab 7.12.0 (The MathWorks Inc., USA).

## 3. Results and discussion

### 3.1. Spectral analysis of EPA and deuterated EPA

As shown in Fig. 1, characteristic bands of EPA-d5 appear in the silent region between 2000 and 2300 $cm^{-1}$. This region is interesting as it does not show vibrational bands for typical organic compounds [14]. It is a region where the tissue and cellular biological matrices do not show bands either.

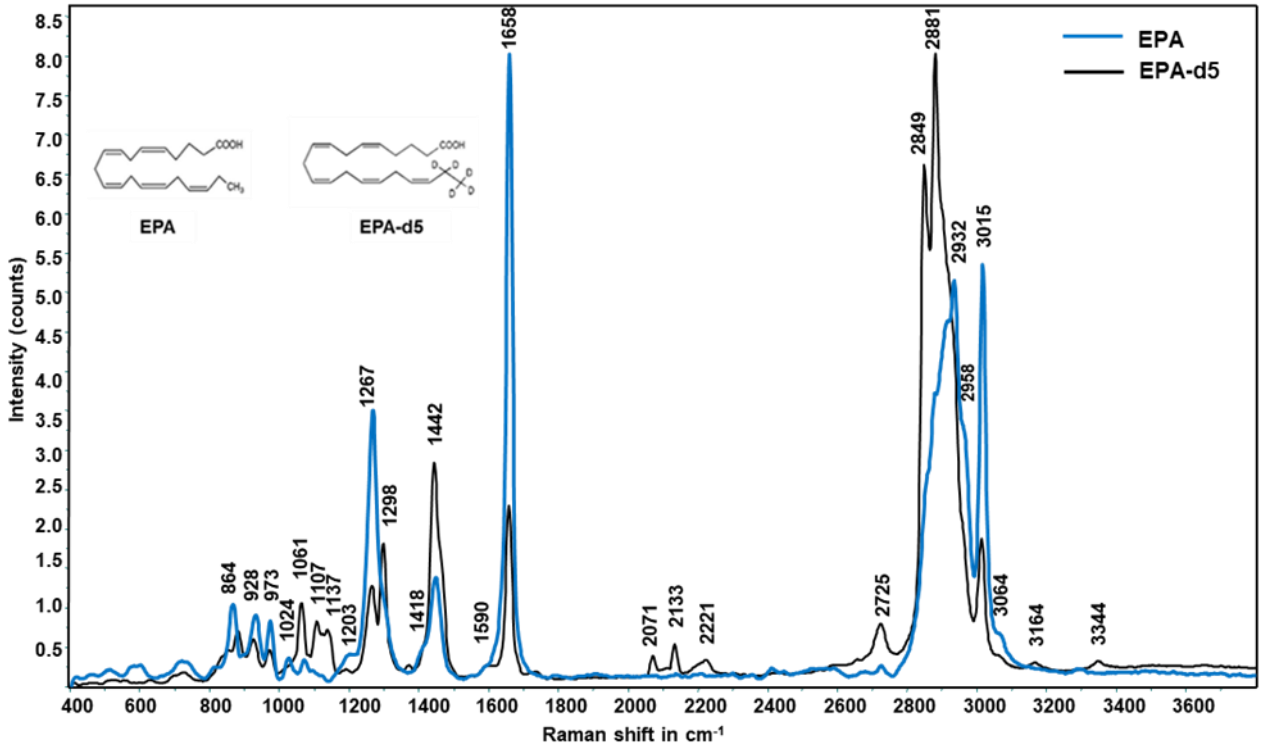


*Fig. 1 Spectral signature and chemical structures of EPA and EPA-d5*

Bands assignment of EPA and EPA-d5 are shown in Table 2. The deuteration generates a shift of the CD bands compared to the CH bands. Indeed, the vibration bands of δ $CH_2$ (1442 $cm^{-1}$), ν $CH_2$ (2849-2881 $cm^{-1}$), $\nu_{sym}$ $CH_3$ (2913 $cm^{-1}$), and $\nu_{asym}$ $CH_3$ (2964 $cm^{-1}$) are shifted to lower wavenumbers after deuteration: δ $CD_2$ (1137 $cm^{-1}$), ν $CD_2$ (2133 $cm^{-1}$), $\nu_{sym}$ $CD_3$ (2071 $cm^{-1}$) and $\nu_{asym}$ $CD_3$ (2221 $cm^{-1}$).

Concerning the carboxyl group, the vibration of the ν C=O stretching is between 1600 and 1800 $cm^{-1}$ and, more precisely, around 1700 $cm^{-1}$ [15]. This is not the case in our recorded spectra. Indeed, Raman spectral signatures recorded on various fatty acids [16] and on EPA [17] do not contain the ν C=O stretching band. On the other hand, the Raman spectrum of deuterated EPA shows some bands of very low intensity around 3164 and 3341 $cm^{-1}$, which can be attributed to the stretching of the OH bond. These bands are not visible on the EPA spectrum [17]. For OH bond and according to the literature, OH bands are better detected in IR, and δ OH appears with a very weak intensity on the Raman spectra of certain fatty acids (around 1590 $cm^{-1}$) [18,19].

The EPA spectrum illustrates a broad and intense band around 1267 $cm^{-1}$, which encompasses the band at 1298 $cm^{-1}$. However, these two bands are distinguished on the EPA-d5 spectrum. An increase in the wavenumber of the ν C-O band from 1094 $cm^{-1}$ to 1107 $cm^{-1}$ is also observed on the EPA-d5 spectrum. Garasevych, et al., observed the same phenomenon for deuterated cytidine and 6-azacytidine and explained it by a modification of the ν C-O band stiffness constant k due to the substitution of intramolecular H bonds by D bonds [20].

*Table 1 Raman bands assignment of each of EPA and EPA-d5 molecules*

| **EPA-band position in $cm^{-1}$** | **Intensity** | **EPA-d5 band position in $cm^{-1}$** | **Intensity** | **Assignment** |
|---|---|---|---|---|
| **864** | m | **881** | w | δ C-C in lipids [21] |
| **928** | m | **926** | w | τ C-H [21] |
| **973** | m | **973** | w | τ C-H [21] |
| **1024** | w | | | δ (C-H) [16] |
| **1068** | w | **1061** | m | ν C-C trans [17] |
| **1094** | w | **1107** | w | ν C-C [16] et ν C-O [15] |
| **1120** | w | **1125** | w | ν C-C trans [16,17] |
| | | **1137** | w | δ $CD_2$ [14] |
| **1267** | s | **1264** | m | δ =C-H *in plane* [17,22] |
| **1298** | m | **1298** | m | τ $CH_2$ [17] |
| **1418** | w | **1417** | m | δ (C-$H_2$) [16] |
| **1447** | m | **1442** | s | $\delta_{sc}$ $CH_2$ [17,21] |
| **1590** | w | **1590** | w | δ OH [18] |
| **1658** | vs | **1658** | s | ν C=C cis [17,21] |
| | | **2071** | w | $\nu_{sym}$ $CD_3$ [14] |
| | | **2133** | w | ν $CD_2$ [14,23] |
| | | **2221** | w | $\nu_{asym}$ $CD_3$ [14] |
| **2725** | w | **2725** | w | ν C-$CH_3$ [22] |
| **2858** | s | **2849** | vs | $\nu_{sym}$ $CH_2$ [16,24] |

| | | | | |
|---|---|---|---|---|
| **2879** | s | **2881** | vs | $\nu_{asym}$ $CH_2$ [16,24] |
| | | **2900** | vs | ternary ν C-H [22] |
| **2913** | s | **2913** | vs | $\nu_{sym}$ $CH_3$ [16,22] |
| **2932** | s | | | $\nu_{sym}$ $CH_3$ [16,22] |
| **2958** | s | | | $\nu_{asym}CH_3$ [16,22] |
| **3015** | s | **3015** | s | ν =C-H [16] |
| **3064** | w | **3064** | | ν CH [25] |
| | | **3164, 3341** | w | ν OH [18,19] |

**Vibration modes:** ν: stretching, $\nu_{sym}$: symmetrical stretching, $\nu_{asym}$: asymmetrical stretching, δ: bending, τ: twisting, $\delta_w$: wagging, $\delta_{sc}$: scissoring. **Intensity** w: weak, m: medium, s: strong, vs: very strong.

### 3.2. Spectral analysis of THP-1 nucleus and cytoplasm spectra

From the spectra of the nucleus and the cytoplasm of each cell, we calculated six average spectra in total: each corresponds to a condition of supplementation. We then proceeded to assign the bands while referring to the team's previous work on the analysis of J774 by Raman vibrational spectroscopy [11]. The spectra are slightly different from one condition to another (Fig. 2), and the characteristic bands due to deuteration appear on the spectrum of the cytoplasm of the cells in the media supplemented with EPA-d5, which confirms its endocytosis.

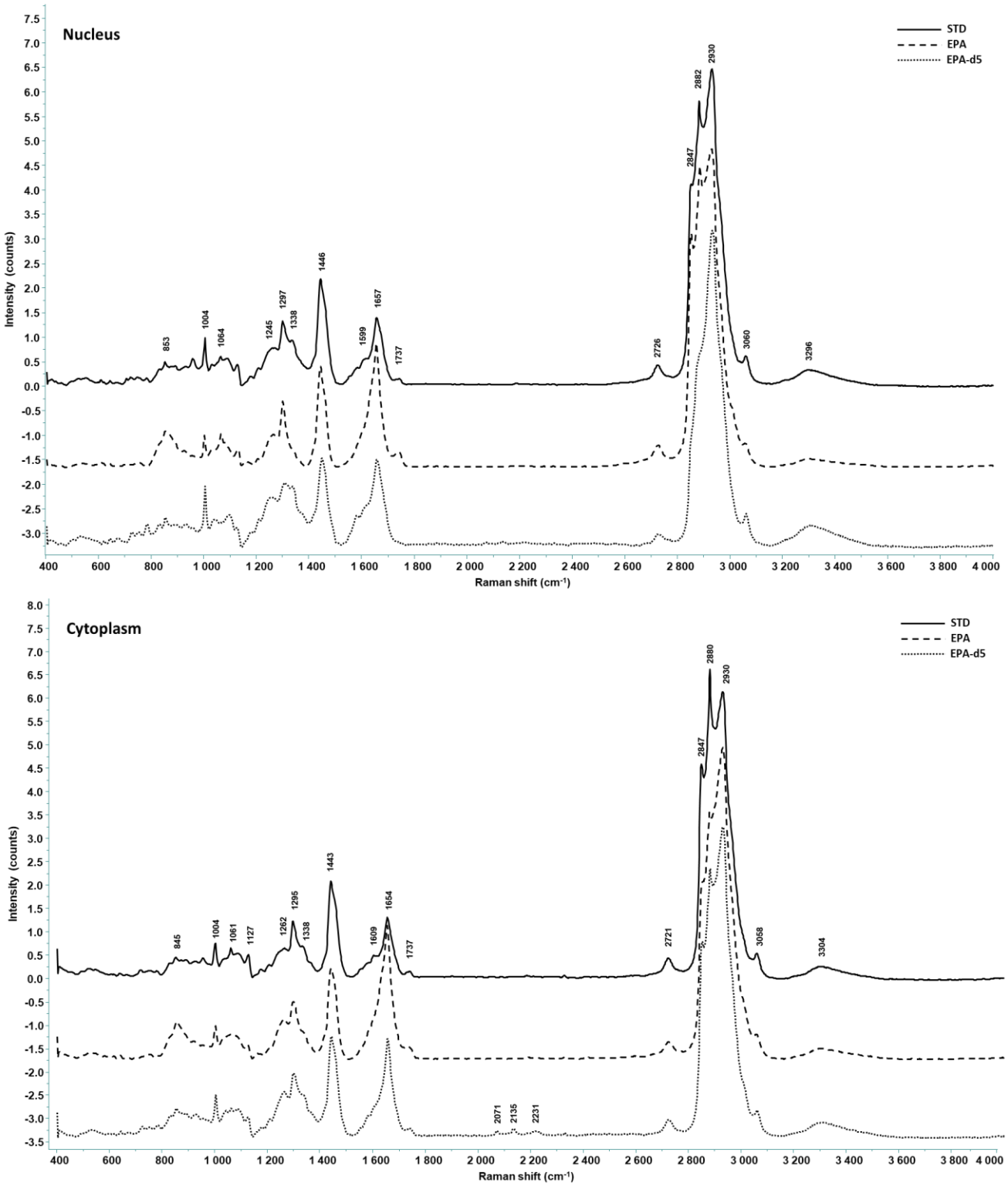


*Fig. 2 Raman spectral signature of nucleus and cytoplasm of THP-1 cells in different conditions of supplementation*

The spectral signature of THP-1 is remarkably close to that of the J774 registered by Tfaili et al. [11], (Fig. S1 in supplementary data). The position of the bands is the same; some differences can be highlighted regarding the shoulder or the intensity ratio of certain bands.

### 3.3. Dimensions and spectral signature of LDs

The number, size, and spectral signature of LDs help in studying the behavior of macrophages in lipid storage. By referring to the visible image of the cells, we extracted the size in µm of each LD (Fig. 3).

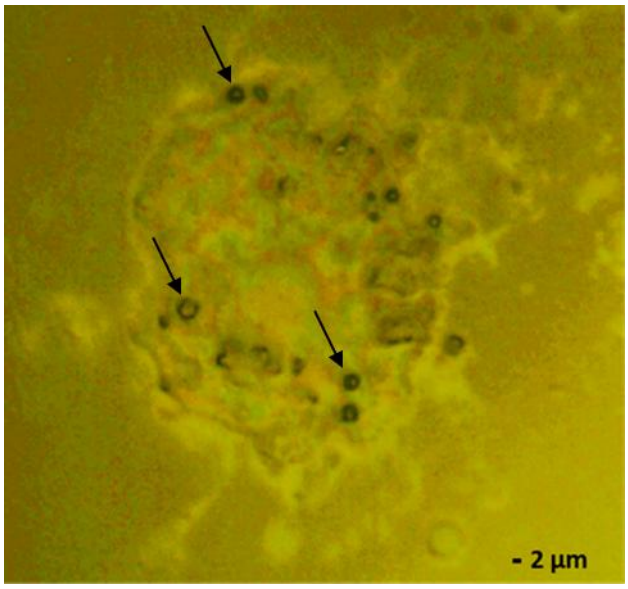


*Fig. 3 THP-1 cell containing lipid droplets (we indicated some LD with black arrows)*

The values for each condition are represented in a box plot in Fig.4. The size of the LDs is reduced during the hydrolysis regardless of the supplementation condition. At the same time, we performed a one-factor analysis of variance (ANOVA) test on the LD dimension data. We firstly considered the hydrolysis time for each medium (STD, EPA, EPA-d5) as the studied factor. Then, we considered the supplementation condition at each hydrolysis time as the studied factor in a second time.

The test indicated a significant reduction in the dimensions of the LDs passing from one hydrolysis time to another. When considering the supplementation condition, the test showed a significant difference between the dimension values for hydrolysis times H0 and H2 and no significant difference for the supplementation at H1. (Table S1 and Table S2 in the supplementary data).

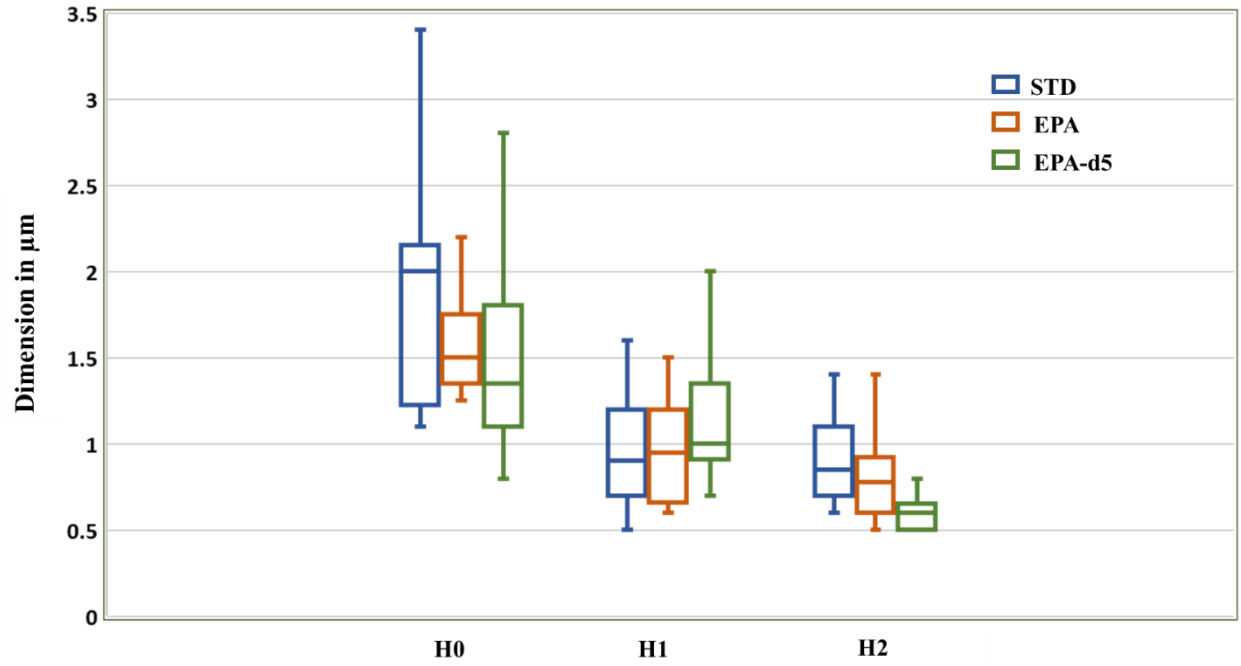


*Fig. 4 Statistical repartition of dimensions of LD with respect to each condition (supplementation condition and hydrolysis time)*

From the spectral signature of LDs, we calculated an average LD spectrum for each culture condition. The characteristic bands of the silent region (2000-2300 $cm^{-1}$) of the deuterated EPA are present in the spectra of the LD present in macrophages supplemented by EPA-d5 [14]. This indicates the incorporation of EPA into the LDs and confirms the origin of the lipid changes.

### 3.4. Spectral signature of lipid droplets without hydrolysis (H0), after 24h (H1), and 48h (H2) of hydrolysis under different supplementation conditions.

We compared the spectral signature of LDs under different culture conditions and at different hydrolysis times. As a reminder, LD consists of a mixture of lipids, essentially cholesterol esters, and triglycerides, surrounded by a membrane of phospholipids [26].

Our results showed that the signature of LDs in STD media differs from that of LDs in media supplemented with EPA or EPA-d5, whose LDs' spectral signatures are similar.

In the fingerprint region without hydrolysis (Fig.5), the 1032 $cm^{-1}$ band assigned to δ ($CH_2$) of fatty acids is less expressed in the STD medium. The intensity and the shouldering of the bands 1032 (δ ($CH_2$) of fatty acids), 1062 (ν(C–C) skeleton lipids), 1085 (ν (CC) lipids), and 1125 $cm^{-1}$ (ν(C–C) lipids: *trans* hydrocarbon chain) [11,16] are similar for EPA and EPA-d5 supplemented media. This expresses a higher FA composition in the droplets of these media and a more abundant lipid composition. The band at 1249 $cm^{-1}$ assigned to ν (P=O) phospholipids [11] is quite distinct on the spectra of LD in STD medium, and it merges with the band at 1263 $cm^{-1}$ attributed to the combination δ (= CH) FA and TG [16] in media

supplemented with EPA and EPA-d5. This result indicates good incorporation of EPA and EPA-d5 in the composition of the FA of the phospholipids. The ratio of the bands 1249 $cm^{-1}$/ 1301 $cm^{-1}$; 1263 $cm^{-1}$/1301 $cm^{-1}$, and 1336 $cm^{-1}$/1301 $cm^{-1}$ – assigned respectively to ν(P=O) phospholipids/δ($CH_2$) lipids; to δ(=CH) fatty acids and TG/δ($CH_2$) lipids and ν (CC) polysaccharides/δ ($CH_2$) lipids [11] – is lower in STD medium indicating more lipids in the LD of media supplemented with EPA and EPA-d5.

In the lipid region (2800-3500 $cm^{-1}$) without hydrolysis (Fig. 6), the band ratio 2932 $cm^{-1}$/ 2876 $cm^{-1}$ assigned to ($\nu_{sym}$ $CH_3$ lipids/ $\nu_{asym}$ $CH_2$ proteins) and the band ratio 2932 $cm^{-1}$/2852 $cm^{-1}$ assigned to ($\nu_{sym}$ ($CH_3$) lipids/ $\nu_{sym}$($CH_2$) lipids) [11] are more intense in media supplemented with EPA and EPA-d5. The band 3011 $cm^{-1}$ assigned to ν (=C-H) of TGs and phospholipids [11] is more visible in the case of STD media. This indicates a high amount of TG in the LDs and confirms a modified lipid composition after supplementation with EPA.

To track the behavior of LDs at different hydrolysis times, we compared the evolution of certain characteristic bands. The bands at 548, 673, and 956 $cm^{-1}$ assigned to the δ($CH_2$) cholesterol, δ(CH), and δ(C=O–C) of fatty acids [16] increased for LD after 24 hours of hydrolysis compared to LD without hydrolysis and then decreased for LD after 48 hours of hydrolysis in the standard medium. This behavior of signals concerning the FA is coupled with two other important behaviors: the successive decrease of the band associated with the ν (>C=O) ester bond of CE and TG [16] at hydrolysis times H1 and H2; and the increase of the intensity of band ν OH from H0 to H1 then its decrease from H1 to H2 but in a way that this band at H2 remains more intense than that to H0 (Fig. 5). These behaviors show the hydrolysis of TG and EC into fatty acids and free cholesterol which causes the variation of the intensity of bands associated with FA and hydroxyl OH function (related to FA, FC, and glycerol). The variation of these bands was more expressed at time H1 than H2, which proves that hydrolysis Kinetics is slowed down beyond 24 hours. This is consistent with the change in the size of the LD (1.87 μm ± 0.59 for 0h, 0.98 μm ± 0.32 for 24h, and 0.88 μm ± 0.23 for 48h of hydrolysis (Fig. 4)). The deceleration in hydrolysis kinetics is due to the decrease in CE and TG over time. Note that the $t_2^1$ of hydrolysis of CE takes 61 hours in THP-1 [27]. In our study, we used a hydrolysis inhibitor (ACAT inhibitor) that blocks only the formation of CE but not the formation of TG. This expresses the decrease in the signal after 24 hours of hydrolysis and then its re-increase for TGs. The TGs are formed by consuming free fatty acids resulting from hydrolysis.

The behavior and ratio of bands at 1126 $cm^{-1}$ (ν(C–C) trans lipids), 1298 $cm^{-1}$ (δ($CH_2$) lipids), 1446 $cm^{-1}$ (δ(C–H) proteins and lipids), 2852 $cm^{-1}$ ($\nu_{asym}$ $CH_2$ lipids), 2932 $cm^{-1}$ ($\nu_{sym}$ $CH_3$ lipids) vary between H0; H1 and H2 of hydrolysis for LDs of the standard medium (Fig. 5,6). This indicates a change in the composition and lipid conformation of the LD. This lipid modification is related to the existence of the hydrolysis process and the resulting efflux of the products. The same behavior is observed for LDs in media supplemented with EPA and EPA-d5.

Differences between LD signals in media supplemented with EPA or EPA-d5 can be highlighted compared to the STD medium. The bands at 673 and 956 $cm^{-1}$ assigned to the

δ(CH) and δ(C=O–C) in FA increased for LD after 24h of hydrolysis compared to LD without hydrolysis, then decreased after 48h of hydrolysis and recorded a lower intensity than that without hydrolysis (Fig. 5). The same behavior is observed at the hydroxyl-OH band (see Fig. 6).

The band associated with ν (>C=O) ester bond of CE and TG decreased at H1 and then increased at H2. All of these behaviors indicate the formation of TG from free fatty acids beyond 24 hours, noting that ACAT inhibitors added to the culture medium are still active. TG formation is more pronounced in LD media supplemented with EPA and EPA-d5 than in the case of STD media. Another clue of the involvement of EPA in the formation of TGs consists in the observed change in the characteristic bands of deuteration in the silent region. As a result of an important amount of TG in LD, we should expect an increase in the LD size in supplemented media. Our results showed that the average size of LD in STD media was higher than in supplemented media at H2 (Fig.4) despite a higher amount of TG. But we noticed that the cells supplemented with EPA or EPA-d5 contain a higher number of LD compared to that found in STD media. The number of LD at H1 and H2 was similar and significantly higher than H0.

To conclude, the hydrolysis kinetics of CE and TG in LD is slowed down beyond 24 hours. This is in accordance with the dimensions of the droplets, which decrease more from H0 to H1 than from H1 to H2. Supplementation with EPA and EPA-d5 promoted TG formation since the inhibitor only blocked the formation of EC.

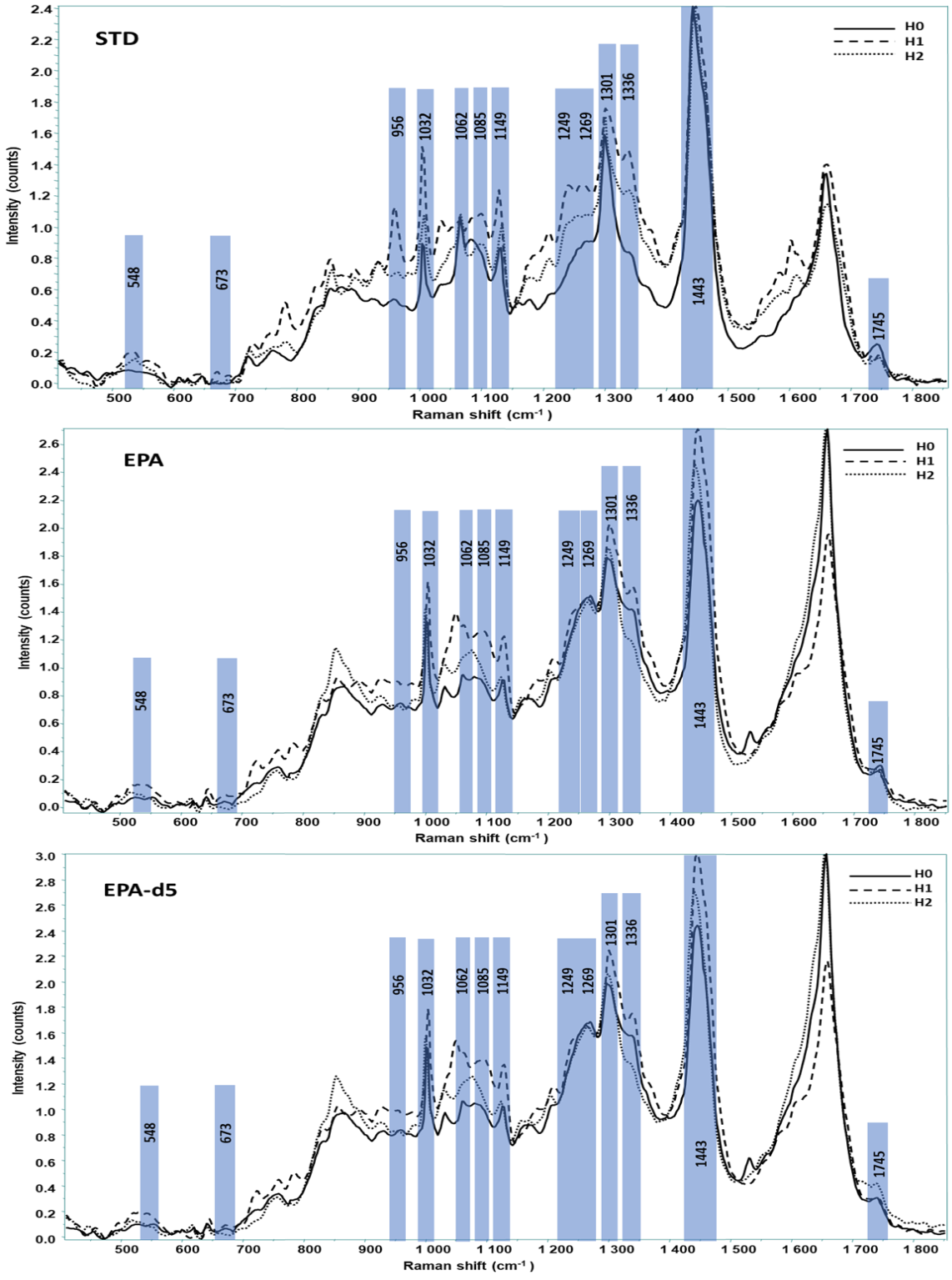


*Fig. 5 Spectral signature of lipid droplets of the spectral region (400-1850 $cm^{-1}$) in the STD medium, the medium supplemented with EPA, and with EPA-d5*

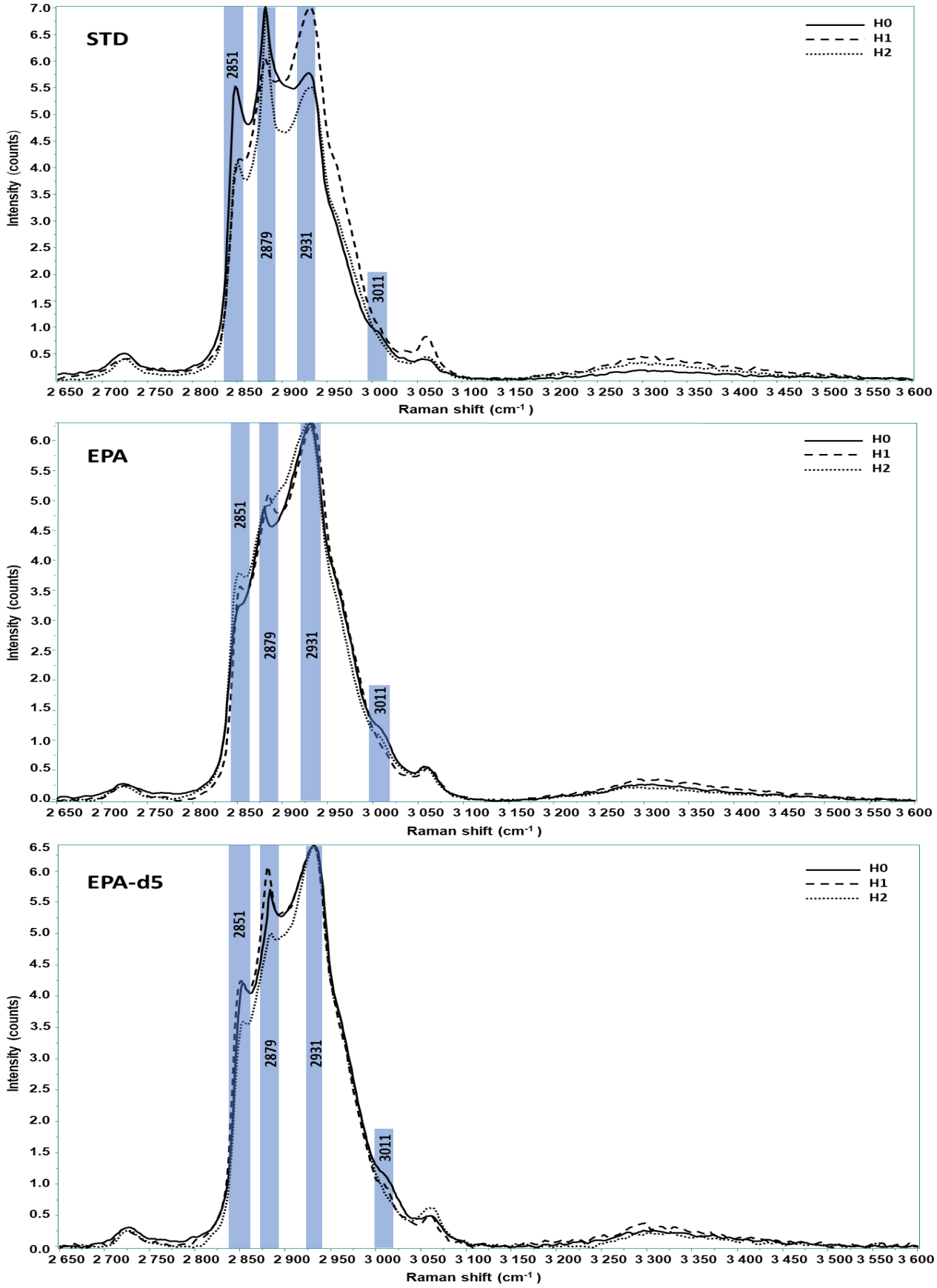


*Fig. 6 Spectral signature of lipid droplets of the spectral region (2650-3600 $cm^{-1}$) in the STD medium, the medium supplemented with EPA, and with EPA-d5*

### 3.5. Principal Component Analysis

Principal component analysis (PCA) was performed on 965 pretreated spectra from the different culture conditions (individuals) and 1865 wavenumbers (variables) after centering and reducing data. As a reminder, these spectra were extracted from LD, cytoplasm, and nuclei. We were interested in the distribution of data according to hydrolysis time (H0, H1, H2), supplementation (STD, EPA, EPA-d5), and according to the type of cell compartment (cytoplasm, nucleus, LD).

The first component represents about 53.3% of the information and the second about 12.4%. The representation of individuals on the score plot on the first two components (PC1 and PC2) may suggest that there are outlier spectra. This is not the case. We checked the preprocessing. The variability is due to the variability within the cell matrix and the large number of spectra. In order to appreciate the distribution of individuals, we have chosen to display the 95% confidence ellipse representing the variability within each group (Fig. S2 in supplementary data).

The projection of individuals on PC1 (53.3%) and PC2 (12.4%) also separates groups between the media of different supplementations (STD, EPA, EPD) according to the second component (PC2) and between hydrolysis times (H0, H1, H2) and cellular compartments (c, n, g) according to the first component (PC1).

The loadings of the first and second components in PCA illustrated bands that allowed us to project data into different groups (Fig. 8). The band at 1061 $cm^{-1}$ assigned to ν(C-C) trans separated the spectra of the medium supplemented with EPA-d5 from the two others. The loading of PC2 also showed that the bands at 864 and 1658 $cm^{-1}$ corresponding to the skeleton ν vibration of lipids and the ν C=C cis permitted to distinguish the spectra of the medium supplemented with EPA. The 750 $cm^{-1}$ band corresponding to DNA characterized the nuclei. The 2225 $cm^{-1}$ band associated with the $\nu_{asym}$ $CD_3$ separated the spectra of the LD due to the effective incorporation of EPA-d5 in the LD and in the cytoplasm. The position of the spectra after 48 hours of hydrolysis (H2) is close to H0. The PCA allowed us to project H0 and H1distinctly from the first two components. The position of H2 between H0 and H1 reflects the increase in the signal observed after 24 hours of hydrolysis and its subsequent decrease after 48 hours while maintaining an overall higher intensity than the spectra at H0.

Bands at 1742 and 2725 $cm^{-1}$ associated with the ν (C=O) of the TG – CE and the ν (C-H) of lipids decreased after 24h of hydrolysis, then increased at 48 hours of hydrolysis while keeping a higher signal than THP-1 without hydrolysis. These bands are negatively correlated with the loading of PC1; this explains the position of H0 spectra in the negative axis dial.

## 4. Conclusion and perspectives

Atherosclerosis is due to the presence of atherosclerotic plaques characterized by cholesterol-laden macrophages called foam cells. In these cells, CE associated with TG form LDs. The only way to eliminate this excess of cholesterol is to promote the efflux of FC from

macrophages to specific acceptors. Fournier et al., recently showed that eicosapentaenoic acid reduces free cholesterol *efflux in vitro* on cholesterol-loaded THP-1 macrophages due to decreased CE hydrolysis. These *in vitro* observations could reflect the EPA's difficulty in facilitating *in vivo* the antiatherogenic process of cholesterol efflux in advanced atherosclerotic plaques.

Herein, we studied *in vitro* the impact of EPA on the hydrolysis of CE of lipid droplets in human THP-1 macrophages. We conducted analyses by Raman vibrational microspectroscopy (which has the advantage of being a non-destructive method) and considered different cell culture conditions: THP-1 overloaded with acetylated LDL in a standard medium (non-supplemented) or in a medium supplemented with EPA or EPA-d5. We also considered the hydrolysis time: without hydrolysis (H0) or after hydrolysis of CE and TG over 24h (H1) or 48h (H2).

Hyperspectral and visible images allowed us to assess the number, size, and location of LDs. The use of deuterium labeling permitted to follow the EPA incorporation based on the characteristic vibrational bands of EPA-d5. Spectral signature helped in evaluating the lipid composition according to the time of hydrolysis. This explains data projection – into groups according to cell compartment (cytoplasm, nucleus, LD), hydrolysis time, and media supplementation – after principal component analysis.

The incorporation of the EPA into the LDs was thus confirmed due to characteristic bands related to deuteration in the silent region (2000-2300 $cm^{-1}$). Lipid droplets decreased in size with hydrolysis time. Hydrolysis Kinetics slowed down beyond 24 hours. This is in accordance with the change in the size of the LD. The latter is more pronounced between H0 and H1 (1.87 µm ± 0.59 for H0, 0.98 µm ± 0.32 for H1) than between H1 and H2 (0.88 µm ± 0.23 for H2).

Spectral signature in STD medium is quite distinct from EPA or EPA-d5 supplemented media. The ratio of bands ν(P=O) phospholipids (1249 $cm^{-1}$) / δ ($CH_2$) lipids (1301 $cm^{-1}$); at δ (=CH) fatty acids and TG (1263 $cm^{-1}$) / δ ($CH_2$) lipids (1301 $cm^{-1}$) and ν (CC) polysaccharides (1336 $cm^{-1}$) / δ ($CH_2$) lipids (1301 $cm^{-1}$) ) is lower in STD medium indicating more lipids in the LDs of EPA and EPA-d5 supplemented media. It is the same for the ratios of bands 2932 $cm^{-1}$ / 2876 $cm^{-1}$ assigned to ($\nu_{sym}$ $CH_3$ lipids / $\nu_{asym}$ $CH_2$ proteins) and bands 2932 $cm^{-1}$ / 2852 $cm^{-1}$ assigned to ($\nu_{sym}$ ($CH_3$) lipids / $\nu_{sym}$($CH_2$ ) lipids) that are more intense in media supplemented with EPA and EPA-d5.

To track the behavior of LD at different hydrolysis times, the monitoring of bands associated with fatty acids (673 and 956 $cm^{-1}$), CE and TG (1742 $cm^{-1}$), and hydroxyl function (-OH) showed that the hydrolysis Kinetics of CE and TG is slowed down beyond 24 hours in all media. Results also highlighted a remarkable formation of TGs from fatty acids in LDs of EPA and EPA-d5 supplemented media. The composition of fatty acids changed and decreased after 48 hours of hydrolysis in EPA supplemented media. We also noticed a slowdown in hydrolysis kinetics after 24 hours, with an increase in TG and a decrease in the intensity of the characteristic bands of deuteration in the silent region. This is in agreement with the assumption that EPA, unlike other PUFAs, reduces the hydrolysis of CE and TGs of LD. In

our study, we blocked the pathway of CE formation from FC, but we did not add an inhibitor to block the pathway for TG formation. In the presence of EPA, the TG amount continued to increase. We should also remind that EPA might also be a part of the composition of phospholipids as specified above.

In perspective, analyses by gas chromatography coupled with mass spectrometry can help in getting the fatty acids composition. Analyses by normal phase liquid chromatography (NPLC) coupled with mass spectrometry can also quantify total lipids composition [28]. In the previous J774 study, chemometric analysis permitted the distinction of the spectral signature of the nucleus and cytoplasm by infrared (IR) imaging despite the fact that a pixel covered an entire cell [11]. THP-1s are somewhat larger than J774 mouse macrophages; we can record IR images and evaluate the ability of chemometric methods to discriminate signatures from the nucleus, cytoplasm, and lipid droplets. The interest lies in the saving of acquisition time between Raman and IR. A comparative study between the changes occurring following supplementation with EPA-d5 of THP-1 and J774 overloaded with acetylated LDL will permit us to evaluate the behavior of each cell line better.

**ACKNOWLEDGMENTS**

*This work has been supported as part of France 2030 programme "ANR-11-IDEX-0003", from the OI HEALTHI of the Université Paris-Saclay.*

## REFERENCES


[1] K.J. Moore, F.J. Sheedy, E.A. Fisher, Macrophages in atherosclerosis: a dynamic balance, Nat Rev Immunol. 13 (2013) 709–721. https://doi.org/10.1038/nri3520.

[2] R.S. Rosenson, H.B. Brewer, W.S. Davidson, Z.A. Fayad, V. Fuster, J. Goldstein, M. Hellerstein, X.-C. Jiang, M.C. Phillips, D.J. Rader, A.T. Remaley, G.H. Rothblat, A.R. Tall, L. Yvan-Charvet, Cholesterol efflux and atheroprotection: Advancing the concept of reverse cholesterol transport, Circulation. 125 (2012) 1905–1919. https://doi.org/10.1161/CIRCULATIONAHA.111.066589.

[3] D.L. Bhatt, P.G. Steg, M. Miller, E.A. Brinton, T.A. Jacobson, S.B. Ketchum, R.T. Doyle, R.A. Juliano, L. Jiao, C. Granowitz, J.-C. Tardif, C.M. Ballantyne, Cardiovascular Risk Reduction with Icosapent Ethyl for Hypertriglyceridemia, N Engl J Med. 380 (2019) 11–22. https://doi.org/10.1056/NEJMoa1812792.

[4] R.P. Mason, P. Libby, D.L. Bhatt, Emerging Mechanisms of Cardiovascular Protection for the Omega-3 Fatty Acid Eicosapentaenoic Acid, ATVB. 40 (2020) 1135–1147. https://doi.org/10.1161/ATVBAHA.119.313286.

[5] H. Dakroub, M. Nowak, J.-F. Benoist, B. Noël, B. Vedie, J.-L. Paul, N. Fournier, Eicosapentaenoic acid membrane incorporation stimulates ABCA1-mediated cholesterol efflux from human THP-1 macrophages, Biochimica et Biophysica Acta (BBA) - Molecular and Cell Biology of Lipids. 1866 (2021) 159016. https://doi.org/10.1016/j.bbalip.2021.159016.

[6] N. Fournier, G. Sayet, B. Vedie, M. Nowak, F. Allaoui, A. Solgadi, E. Caudron, P. Chaminade, J.-F. Benoist, J.-L. Paul, Eicosapentaenoic acid membrane incorporation impairs cholesterol efflux from cholesterol-loaded human macrophages by reducing the cholesteryl ester mobilization from lipid droplets, Biochimica et Biophysica Acta (BBA) - Molecular and Cell Biology of Lipids. 1862 (2017) 1079–1091. https://doi.org/10.1016/j.bbalip.2017.07.011.

[7] C. Stiebing, L. Schmölz, M. Wallert, C. Matthäus, S. Lorkowski, J. Popp, Raman imaging of macrophages incubated with triglyceride-enriched oxLDL visualizes translocation of lipids between endocytic vesicles and lipid droplets, Journal of Lipid Research. 58 (2017) 876–883. https://doi.org/10.1194/jlr.M071688.

[8] K. Majzner, S. Chlopicki, M. Baranska, Lipid droplets formation in human endothelial cells in response to polyunsaturated fatty acids and 1-methyl-nicotinamide (MNA); confocal Raman imaging and fluorescence microscopy studies, J. Biophoton. 9 (2016) 396–405. https://doi.org/10.1002/jbio.201500134.

[9] C. Stiebing, C. Matthäus, C. Krafft, A.-A. Keller, K. Weber, S. Lorkowski, J. Popp, Complexity of fatty acid distribution inside human macrophages on single cell level using Raman micro-spectroscopy, Anal Bioanal Chem. 406 (2014) 7037–7046. https://doi.org/10.1007/s00216-014-7927-0.

[10] C. Matthäus, C. Krafft, B. Dietzek, B.R. Brehm, S. Lorkowski, J. Popp, Noninvasive Imaging of Intracellular Lipid Metabolism in Macrophages by Raman Microscopy in Combination with Stable Isotopic Labeling, Anal. Chem. 84 (2012) 8549–8556. https://doi.org/10.1021/ac3012347.

[11] S. Tfaili, A. Al Assaad, N. Fournier, F. Allaoui, J.-L. Paul, P. Chaminade, A. Tfayli, Investigation of lipid modifications in J774 macrophages by vibrational spectroscopies after eicosapentaenoic acid membrane incorporation in unloaded and cholesterol-loaded cells, Talanta. 199 (2019) 54–64. https://doi.org/10.1016/j.talanta.2019.01.122.

[12] At the Cell Counter: THP-1 Cells., (2022). https://www.moleculardevices.com/applications/cell-counting/cell-counter-thp-1-cells (accessed May 31, 2022).

[13] S. Chitra, G. Nalini, T. Lokeswari, Comparison of differentiation to macrophages in isolated monocytes from human peripheral blood and THP1 cells," *Sri Ramachandra Journal of Medicine*, 7 (2014). https://www.sriramachandra.edu.in/university/pdf/research/journals/july_2015/comparison-of.pdf.
[14] K.A. Okotrub, D.V. Shamaeva, N.V. Surovtsev, Raman spectra of deuterated hydrocarbons for labeling applications, J Raman Spectroscopy. 53 (2022) 297–309. https://doi.org/10.1002/jrs.6279.
[15] H. Wu, J.V. Volponi, A.E. Oliver, A.N. Parikh, B.A. Simmons, S. Singh, In vivo lipidomics using single-cell Raman spectroscopy, Proc. Natl. Acad. Sci. U.S.A. 108 (2011) 3809–3814. https://doi.org/10.1073/pnas.1009043108.
[16] K. Czamara, K. Majzner, M.Z. Pacia, K. Kochan, A. Kaczor, M. Baranska, Raman spectroscopy of lipids: a review: Raman spectroscopy of lipids, J. Raman Spectrosc. 46 (2015) 4–20. https://doi.org/10.1002/jrs.4607.
[17] P. Meksiarun, N. Spegazzini, H. Matsui, K. Nakajima, Y. Matsuda, H. Sato, In vivo study of lipid accumulation in the microalgae marine diatom Thalassiosira pseudonana using Raman spectroscopy, Appl Spectrosc. 69 (2015) 45–51. https://doi.org/10.1366/14-07598.
[18] R.L. Frost, Y. Xi, R.E. Pogson, Raman spectroscopic study of the mineral arsenogorceixite BaAl3AsO3(OH)(AsO4,PO4)(OH,F)6, Spectrochimica Acta Part A: Molecular and Biomolecular Spectroscopy. 91 (2012) 301–306. https://doi.org/10.1016/j.saa.2012.02.011.
[19] T. Ohtani, Y. Ohno, S. Sasaki, T. Kume, H. Shimizu, High-pressure Raman study of methane hydrate "filled ice," J. Phys.: Conf. Ser. 215 (2010) 012058. https://doi.org/10.1088/1742-6596/215/1/012058.
[20] S. Garasevych, M. Iakhnenko, O. Slobodyanyuk, I. Vaskivskyi, Abnormal shifts in Raman spectra of deuterated cytidine and 6-azacytidine, Spectroscopy. 24 (2010) 191–195. https://doi.org/10.1155/2010/107694.
[21] D.P. Killeen, A. Card, K.C. Gordon, N.B. Perry, First Use of Handheld Raman Spectroscopy to Analyze Omega-3 Fatty Acids in Intact Fish Oil Capsules, Appl Spectrosc. 74 (2020) 365–371. https://doi.org/10.1177/0003702819877415.
[22] A. Tfayli, E. Guillard, M. Manfait, A. Baillet-Guffroy, Thermal dependence of Raman descriptors of ceramides. Part I: effect of double bonds in hydrocarbon chains, Anal Bioanal Chem. 397 (2010) 1281–1296. https://doi.org/10.1007/s00216-010-3614-y.
[23] C. Stiebing, T. Meyer, I. Rimke, C. Matthäus, M. Schmitt, S. Lorkowski, J. Popp, Real-time Raman and SRS imaging of living human macrophages reveals cell-to-cell heterogeneity and dynamics of lipid uptake, J. Biophoton. 10 (2017) 1217–1226. https://doi.org/10.1002/jbio.201600279.
[24] S. TFAILI, Caractérisation par microspectroscopie confocale Raman de la diffusion cutanée d'actif : optimisation des paramètres instrumentaux et méthodologiques en vue d'applications in vivo., n.d. http://www.theses.fr/2012REIMP203.
[25] K. Kachrimanis, D.E. Braun, U.J. Griesser, Quantitative analysis of paracetamol polymorphs in powder mixtures by FT-Raman spectroscopy and PLS regression, Journal of Pharmaceutical and Biomedical Analysis. 43 (2007) 407–412. https://doi.org/10.1016/j.jpba.2006.07.032.
[26] A. Castoldi, L.B. Monteiro, N. van Teijlingen Bakker, D.E. Sanin, N. Rana, M. Corrado, A.M. Cameron, F. Hässler, M. Matsushita, G. Caputa, R.I. Klein Geltink, J. Büscher, J. Edwards-Hicks, E.L. Pearce, E.J. Pearce, Triacylglycerol synthesis enhances macrophage inflammatory function, Nat Commun. 11 (2020) 4107. https://doi.org/10.1038/s41467-020-17881-3.

[27] A.T. Lada, M.C. Willingham, R.W. St Clair, Triglyceride depletion in THP-1 cells alters cholesteryl ester physical state and cholesterol efflux, J Lipid Res. 43 (2002) 618–628.
[28] S. Abreu, A. Solgadi, P. Chaminade, Optimization of normal phase chromatographic conditions for lipid analysis and comparison of associated detection techniques, Journal of Chromatography A. 1514 (2017) 54–71. https://doi.org/10.1016/j.chroma.2017.07.063.